Green Synthesized Fe₃O₄ Nanoparticles as Silymarin Drug Carrier and their Anticancer Activity against Liver-HepG2 and Lung-A549 Cancer Cells

J. Manikandan[1,*], P. Rajesh[2], J. Raffiea Baseri[1] and S.V.K. Selvakumar[2]

[1]Department of Chemistry, P.S.G. College of Arts & Science, Coimbatore-641 014, India
[2]Department of Chemistry, Government Arts College, Coimbatore-641018, India

*Corresponding author: E-mail: alphachemtution@gmail.com

Iron oxide nanoparticles (IONPs) were synthesized by co-precipitation method with *Commiphora berryi* latex as stabilizing agent. The IONPS were coated with PEG2K and then loaded with silymarin drug. The synthesized IONPs, PEG2K and silymarin loaded nanoparticles were analyzed by FTIR, XRD, SEM and TEM techniques. The FTIR results indicated the coating of plant materials and the drug on the nanoparticles. The XRD results showed that the synthesized particles have a crystalline structure and controlled size of about 14.5 nm. Surface morphology of the iron oxide nanoparticles and drug loaded IONPs from SEM and TEM results show the cubic shaped particles with less agglomeration. The silymarin loaded IONPs were tested against liver and lung cancer cells by MTT assay and fluorescence microscopic analysis using various concentrations such as 10 µL, 25 µL and 50 µL. Results confirmed that the cell apoptosis was done by nucleus fragmentations. Further, the quantitative cell apoptosis was done by flow cytometric method. The results confirmed that the silymarin loaded IONPs disclosed excellent anticancer activity against lung cancer cells with 30.47% of post apoptotic cells over liver cancer cells with 30.27% post apoptosis.

Keywords: Iron oxide nanoparticles, Silymarin, Fluorescence, Flow cytometric, Cytotoxic analysis, A549 and HepG2 cancer cells.

INTRODUCTION

Cancer is one of the most devastating diseases which can affect any individual at any stage and develop in any organ of the body. According to World health report, more than 10 million new cancer cases and cancer-related deaths are annually reported. Lung cancer and liver cancer are associated with the greatest mortality rate compared to other types of cancer. The populations of Africa, Asia and Central and South America represent 70% of all cancer deaths and 60% of the total new annual cancer cases worldwide [1]. Among the different types of therapies, chemotherapy is the most commonly used technique which involves the use of alkylating agents, antimetabolites and plant products.

There are various undesirable side effects of chemotherapy alone or in combination with cytotoxic drug therapy or radiation therapy [2]. Chemotherapeutics are not always effective in depleting malignant cells and the exponential mortality rate among cancer patients and also have side effects such as multi drug resistance. One of the novel methodologies for the treatment of cancer is usage of nanomaterial as carriers of anticancer drugs. The drug delivery by nano materials has led to the controlled release of the anticancer drugs and enhanced their activity *in vivo* efficacy [3].

In recent decades, inorganic magnetic core shell nanoparticles (MNPs) as the fascinating area of green chemistry have received considerable attention using environmentally safe reagents and clean synthetic procedures [4]. Studies on various nanomaterials have shown that magnetic nanoparticles (MNPs) as an ecofriendly metal oxides have great potential in modern medical applications, including controlled drug and gene delivery systems and improve medical effect of cancer therapy *via* magnetic hyperthermia and radiotherapy methodologies [5].

Iron oxide nanoparticles (IONPs) are considered as the foremost nano scale materials among various other nanoparticles because of their low cost, super paramagnetic behaviour, biocompatibility with low cytotoxicity and biodegradability

[6]. Also, these nanoparticles have many practical applications such as ferro fluids, biosensors, catalysts, separation processes and environmental remediation. Because of their super paramagnetic property, IONPs are considered as better target agents when exposed to an external magnetic field and are also the only metal oxide nanoparticles approved for use in MRI. The most important feature of IONPs is their ability to add together with different biological molecules like peptides, enzymes, nucleic acids, lipids, fatty acids and various metabolites. Therefore, attempts were made to synthesis of iron oxide nanoparticles (IONPs) using plant extracts.

Several chemical, physical and biological methods have been employed for the synthesis of IONPs. Chemical synthesis generally comprises of co-precipitation, flow injection, microemulsion techniques, reverse micelles, sol-gel synthesis and hydrothermal reactions [7]. The production of Fe_3O_4 nanoparticles using aqueous *Kappaphycus alvarezii* (red seaweed) was studied by Arularasu *et al.* [8]. The degradation of textile waste by catalytic activity was effective using nanoparticles formed by a reduction reaction and also exhibited antibacterial activity. Iron oxide nanoparticles using ethanolic extract of *Centella asiatica* (CAIONPs) by reducing ferrous and ferric chlorides which were administered to Swiss albino mice with a dosage of 2000 mg/kg body weight. No effects of nanoparticles on various tissues were revealed by histopathological studies, indicating that green synthesized nanoparticles were safe for use in biomedical and drug delivery systems [9]. Because of the presence of phytochemical and bioactive compounds, the plant extracts play a significant role in the formation, capping, and stabilization of iron(II) oxide nanoparticles. Due to the presence of polyphenols and antioxidants, the extracts shield the nanoparticles from oxidation and aggregation and this process was highly demanding [10].

Silymarin chemically is (5,7-trihydroxy-2-[3-(4-hydroxy-3-methoxyphenyl)-2-(hydroxy-methyl)-1,4-benzodioxan-6-yl]-4-chromanone), one of the best known hepatoprotective drugs obtained from the seeds of *Silybum marianum* L. (Family: Asteraceae or Compositae). This plant known as milk thistle is being used as an herbal cure for liver and biliary tract diseases. This plant has also been known to safeguard and regenerate the liver cells in various diseases affecting liver such as cirrhosis, jaundice and hepatitis. It exhibits strong antioxidant action via free radical scavenging activity and inhibits lipid peroxidation [11,12].

In present investigation, iron oxide nanoparticles (IONPs) were synthesized by co-precipitation method using *Commiphora berryi* gum as stabilizing agent and then PEG2K coated followed by silymarin drug loading. The synthesized nanoparticles are functionally characterized by using different techniques such as FTIR, XRD, SEM and TEM analysis. Finally, the iron oxide nanoparticles were investigated for the anticancer activity against HepG2 liver cancer and A549 lung cancer cells.

EXPERIMENTAL

The chemicals ferric chloride hexahydrate ($FeCl_3·6H_2O$), ferrous chloride tetrahydrate ($FeCl_2·4H_2O$), polyethylene glycol (PEG2K) and silymarin were purchased from Merck. The plant latex was collected from a matured *Commiphora berryi* plant, which are abundantly available in and around Namakkal, India and the plant specimen has been authenticated by Tamil Nadu Agricultural University, Coimbatore, India. Plant latex was collected by tapping method by making a deep cut on the barks and stored in 4 ºC for further usage.

Synthesis of Iron oxide nanoparticles (IONPs): The IONPs were synthesized by co-precipitation method [13]. In 100 mL beaker, NH_4OH solution was heated along with an ethanolic solution of *Commiphora berryi* latex at 90 ºC. To this, a hot solution of Fe(II)/Fe(III) mixture was added slowly with vigorous stirring for about 10 min and pH of the solution was adjusted to 11 [14]. The black precipitate of IONPs formed were separated using a magnet, washed with distilled water until no traces of NH_4OH, dried in an oven for 1 h at 90 ºC and then stored.

Preparation of PEG2K loaded IONPs: Exactly 0.3 g of Fe_3O_4 nanoparticles and 0.6 g of PEG2K were dissolved in 50 mL of deionized water using a magnetic stirrer for 15 min [15]. The prepared blend was then sonicated for 2 h at room temperature for uniform dispersion and disaggregation of nanoparticles. Resultant Fe_3O_4@PEG2K particles were separated using a magnet and washed with doubly distilled water to remove excess of uncoated PEG molecules. The sample prepared was then heated for 24 h at 200 ºC in an oven.

Preparation of silymarin-loaded IONPs: Silymarin (25 mg) was dissolved in 5 mL ethanol and 50 mg Fe_3O_4@PEG2K was added into the drug solution and stirred for 20 h to prepare 5 mg/mL of drug-nanoparticle solution. The silymarin-loaded Fe_3O_4@PEG2K were separated by centrifugation and then washed with deionized water. The drug encapsulated nanoparticles were dried at 30 ºC for 12 h [16]. Similarly, solutions of 15 mg/mL and 5 mg/mL drug-nanoparticle were prepared for further use.

Characterization: Surface functionalization of plant latex, PEG2K and silymarin on the iron oxide surface was studied by FTIR with the wavenumber range of 4000 to 400 cm^{-1}. The XRD method was used to study the crystalline nature and the phase identification. Surface morphology and particle size of the prepared nanoparticles were analyzed by SEM and TEM techniques.

Silymarin loading, encapsulation efficiency and *in vitro* drug delivery: Silymarin loaded nanoparticles (5 mg) was dispersed in 10 mL of phosphate buffer solution (PBS) and centrifuged for 30 min at 12,000 rpm [17]. Standard curve was obtained with various dilutions of silymarin and their absorbance was measured at 228 nm using UV spectrophotometer. The unloaded silymarin was determined by measuring the concentration of drug in supernatant after centrifugation and comparing the absorbance from the standard curve. The entrapment efficiency and drug loading efficiency was calculated using eqns. 1 and 2:

$$\text{Encapsulation efficiency (\%)} = \frac{W_0}{W_1} \times 100 \qquad (1)$$

$$\text{Drug loading efficiency (\%)} = \frac{W_0}{W} \times 100 \qquad (2)$$

where, W_0 is the amount of silymarin loaded in the IONPs, W is the amount of IONPs, and W_1 is the amount of silymarin initially added.

Drug releasing profile of silymarin loaded IONPs was investigated by dialysis method at different pHs namely 7.4, 6.8 and 5.5 [18]. The silymarin loaded IONPs were transferred into a dialysis bag and immersed in 95 mL of PBS at pH 5.5, 6.8 and 7.4 under continuous agitation. At constant time intervals, 5 mL of aqueous solution was withdrawn and replaced with 5 mL of fresh PBS. The amount of drug release was estimated by measuring the absorbance at 228 nm for silymarin using UV-visible spectrophotometer at 37 ºC.

MTT assay cytotoxic effect: MTT assay method was used to study the cell viability, by measuring the cells ability to convert MTT to the formazan dye. In a 96-well tissue culture, cells were seeded for 24 h such as 2.5×10^3 cells in each well. The wells were incubated with different concentrations of IONPs, silymarin and silymarin loaded IOPNs for various time periods. About 200 µL of MTT solution was added in the wells and treated for another 5 h. The formed formazan salt was dissolved with 150 µL of DMSO. By measuring the absorbance at 570 nm, the cell growths were studied with the intensity of formazan solution using a 96 well microplate reader.

Acridine orange/ethidium bromide staining and DAPI staining fluorescence methods: Exactly 1 µL of acridie orange and ethidium bromide solutions was mixed with 9 mL of cancer cell suspensions. Cells were washed with phosphate buffer solution and stained with acridie orange and ethidium bromide mixture and incubated for 2 min. After that, the cells were washed with phosphate buffer solution and pictured under fluorescence microscope. The same procedure was followed for DAPI staining method.

Apoptotic cell death analysis: Cell apoptotic effect of IONPs, silymarin and silymarin loaded IONPs were determined by propidium iodide staining flow cytometric method. Cells were incubated for 6 h with IONPs, silymarin and silymarin loaded IONPs and washed with phosphate buffer solution then treated with trypsion/EDTA solution. The cell suspensions were centrifuged at 500 rpm for 10 min. To the cells, 100 µL of annexin V-FITC solution was added and incubated further for 15 min. The cells were then examined with flow cytometer.

RESULTS AND DISCUSSION

FTIR studies: The FTIR of *Commiphora berryi* latex and *Commiphora berryi* latex coated iron oxide nanoparticles are shown in Fig. 1. FTIR spectrum of iron oxide nanoparticle shows a characteristic peak at 578 cm⁻¹ for Fe-O bond which confirms the formation of iron oxide nanoparticles [19]. A broad peak at 3270 cm⁻¹ is due to the presence of -O–H stretching vibration of phenolic compounds and N-H stretching vibration of amino acids [20]. Appearance of a doublet around 2926 cm⁻¹ and 2864 cm⁻¹ confirms the existence of lipid molecules in the latex [21]. Presence of strong peak at 1031 cm⁻¹ is due to C-O bond on flavonols. The band at 1641 cm⁻¹ is due to N-H bending and band at 1372 cm⁻¹ is due to C–N stretching found in the proteins [22,23]. The carbohydrates showed character-
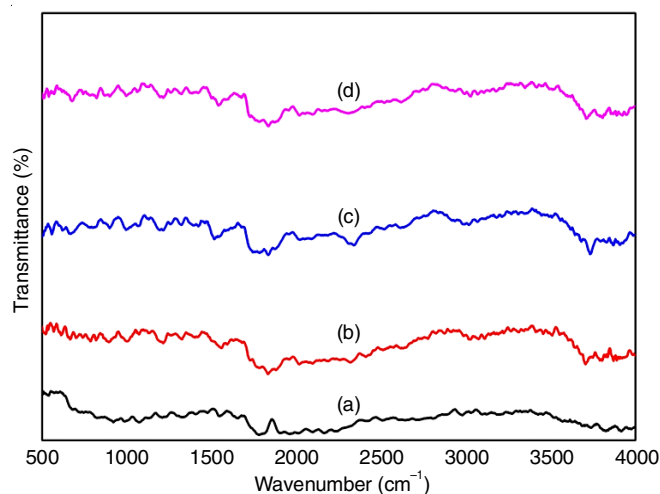

Fig. 1.   FTIR spectra of (a) *Commiphora berryi* latex, (b) IONPs, (c) PEG2K coated IONPs and (d) silymarin loaded IONPs

istic vibration at 1247 cm⁻¹ and 1726 cm⁻¹, which are attributed to -C-O-C- stretching and -C=O stretching respectively.

The peaks correspond to flavonoids and proteins were also observed in IONPs. The absence of –OH vibrations suggested that the IONP cores were protected from the solvation of water molecules by latex layer, which adsorbed on the surface of the IONPs. In the FTIR spectrum of IONP@PEG2K peaks at 2887 cm⁻¹ corresponded to the -CH₂ stretching, 1114 cm⁻¹ was assigned to the -C-O- vibration, 963 cm⁻¹ was due to -C-C- stretching and 3429 cm⁻¹ was attributed to the -OH stretching.

The FTIR spectrum of silymarin loaded IONPs@PEG2K showed a peak at 3890-3500 cm⁻¹ which is due to the –OH stretching, while the peaks at 1627 cm⁻¹, 1602 cm⁻¹ and 1509 cm⁻¹ were attributed to the -C=O, -C=C-, -C-O-C- stretching vibrations, respectively. These results showed that there exists an interaction between PEG2K and silymarin with IONPs.

X-ray diffraction studies: The X-ray diffraction pattern of IONPs (Fig. 2) has six diffraction peaks with 2θ values of 30.56º, 35.86º, 43.48º, 53.86º, 57.63º and 62.71º, which are the characteristic peaks of the crystallographic planes (220), (311), (400), (422), (511) and (440), respectively. These diffraction peaks correspond to the diffraction peaks of Fe₃O₄
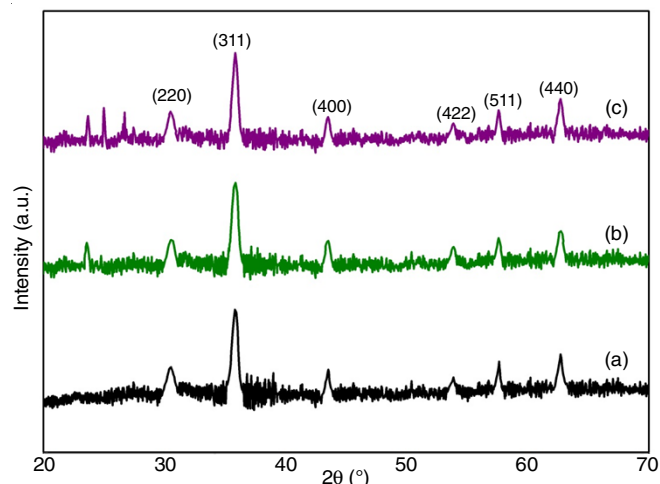

Fig. 2.   X-ray diffraction patterns of (a) IONPs, (b) PEG coated and (c) silymarin loaded IONPs

according to JCPDS Card No. 88-0315. From Fig. 2, it was confirmed that the PEG2K coated and silymarin loaded IONPs were crystalline in nature. The appearance of new peaks in the PEG coated and silymarin loaded IONPs may be due to the adsorption of PEG2K and drug on the surface of nanoparticles and it increased the average crystalline size of IONPs. The crystalline sizes corresponds to the sharp diffraction peak (311) were 14.5 nm 16.8 nm and 18.1 nm respectively for IONPs, PEG2K coated and drug loaded IONPs.

Morphological studies: The comparison of different SEM images in Fig. 3 exhibited a difference in the surface morphology of the synthesized iron oxide nanoparticles, PEG2K coated and drug loaded IONPs. The morphological size variations of the synthesized PEG2K coated and drug loaded IONPs nanoparticles were found to be insignificant while the increase in the size of nanoparticles confirmed the entrapment of PEG2K and silymarin on IONPs. Further, it is seen from the SEM results that the particle aggregation is reduced with PEG2K and silymarin loading.

TEM micrographs of IONPs displayed monodispersed particles with a cubic morphological appearance as shown in Fig. 4. While upon addition of PEG2K and silymarin, the agglomeration of the particles were found to be decreased, which confirmed the prediction from SEM analysis.
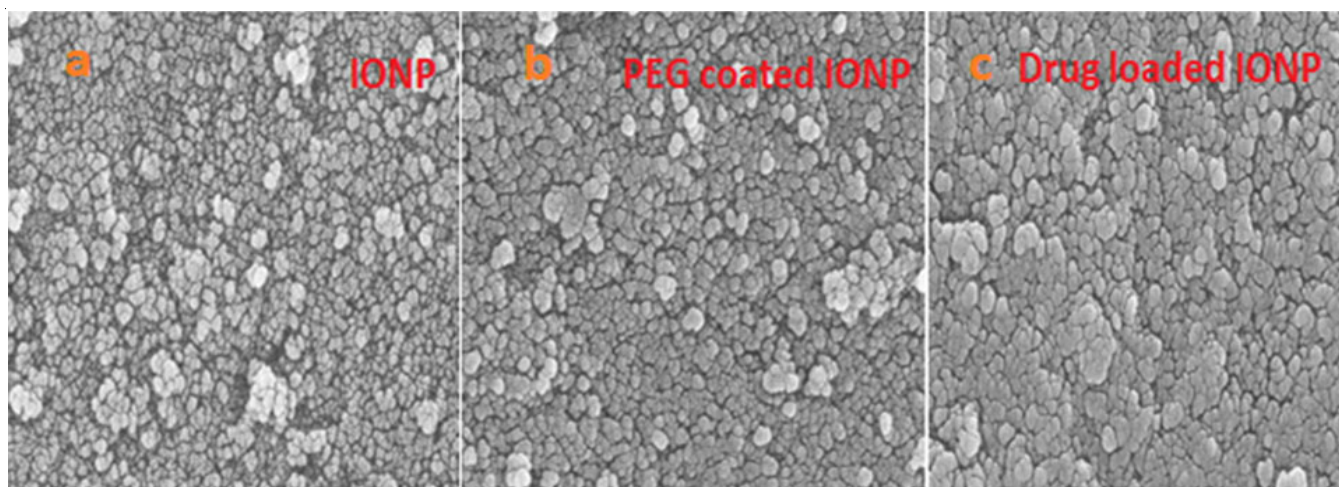

Fig. 3. SEM images of (a) IONPs, (b) PEG coated IONPs and (c) silymarin loaded IONPs
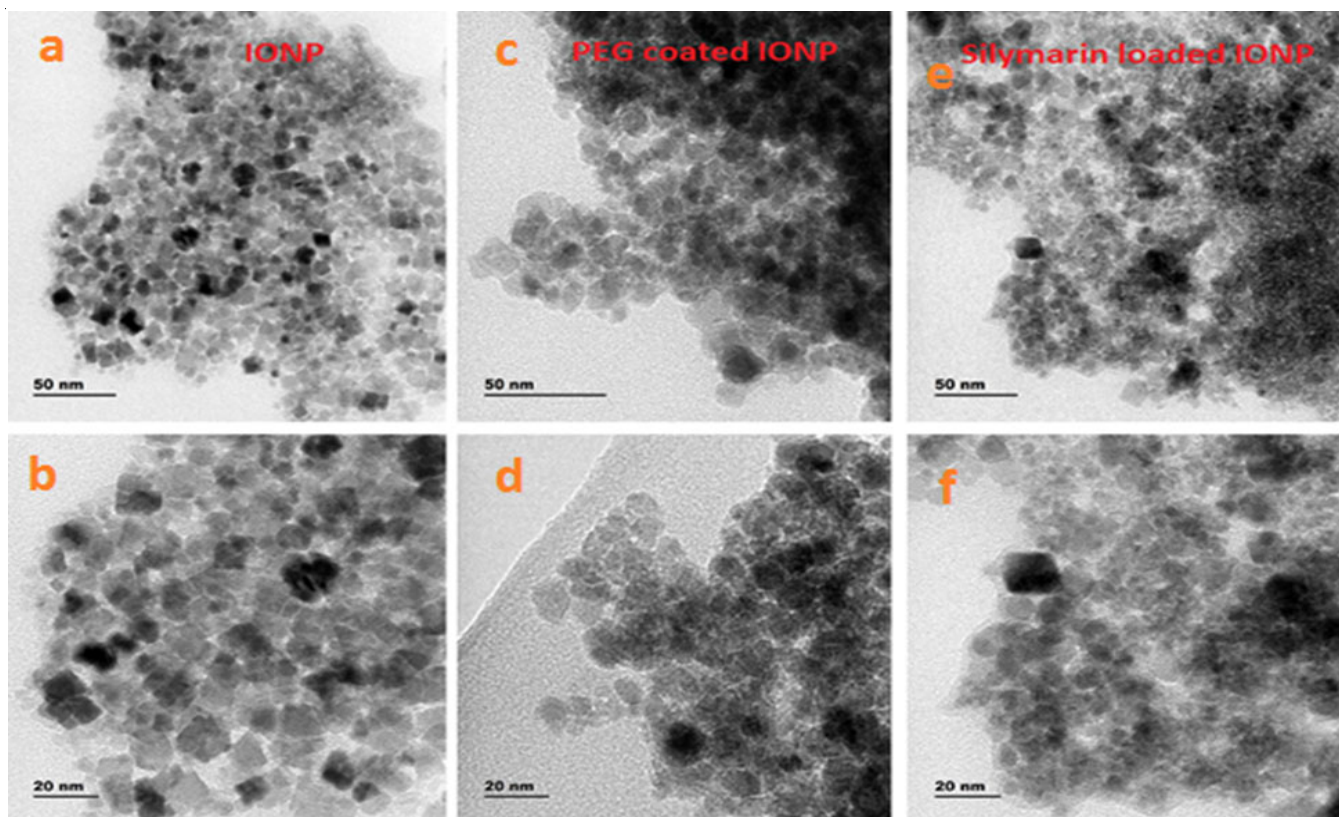

Fig. 4. TEM images of IONPS (a,b), PEG coated IONPs (c,d) and silymarin loaded IONPs (e,f)

Silymarin loading, encapsulation efficiency and *in vitro* drug delivery: The drug loading and encapsulation efficiency with different concentrations are shown in Table-1. The nanoparticles with 5 mg/mL concentration of silymarin exhibits the highest loading and encapsulation efficiency as 5.8% and 67.7%, respectively and thus, can be used for *in vitro* drug release studies. The *in vitro* silymarin release profile is shown in Fig. 5, which clearly depicted that more than about 72% of the entrapped drug was released from the IONPs within 48 h in PBS (pH 5.5). At pH 7.4 and 6.8, drug release ratio was comparably lower than that at pH 5.5.

Fig. 5. *In vitro* silymarin release profile at different pH

TABLE-1
DRUG LOADING AND ENCAPSULATION EFFICIENCY OF SILYMARIN LOADED IONPs

Drug concentration	1 mg/mL	3 mg/mL	5 mg/mL
Drug loading efficiency	2.6	7.1	9.1
Encapsulation efficiency	19.4	68.1	89

MTT assay cytotoxic effect: The effect of IONPs, silymarin and silymarin loaded IONPS on the cell response of
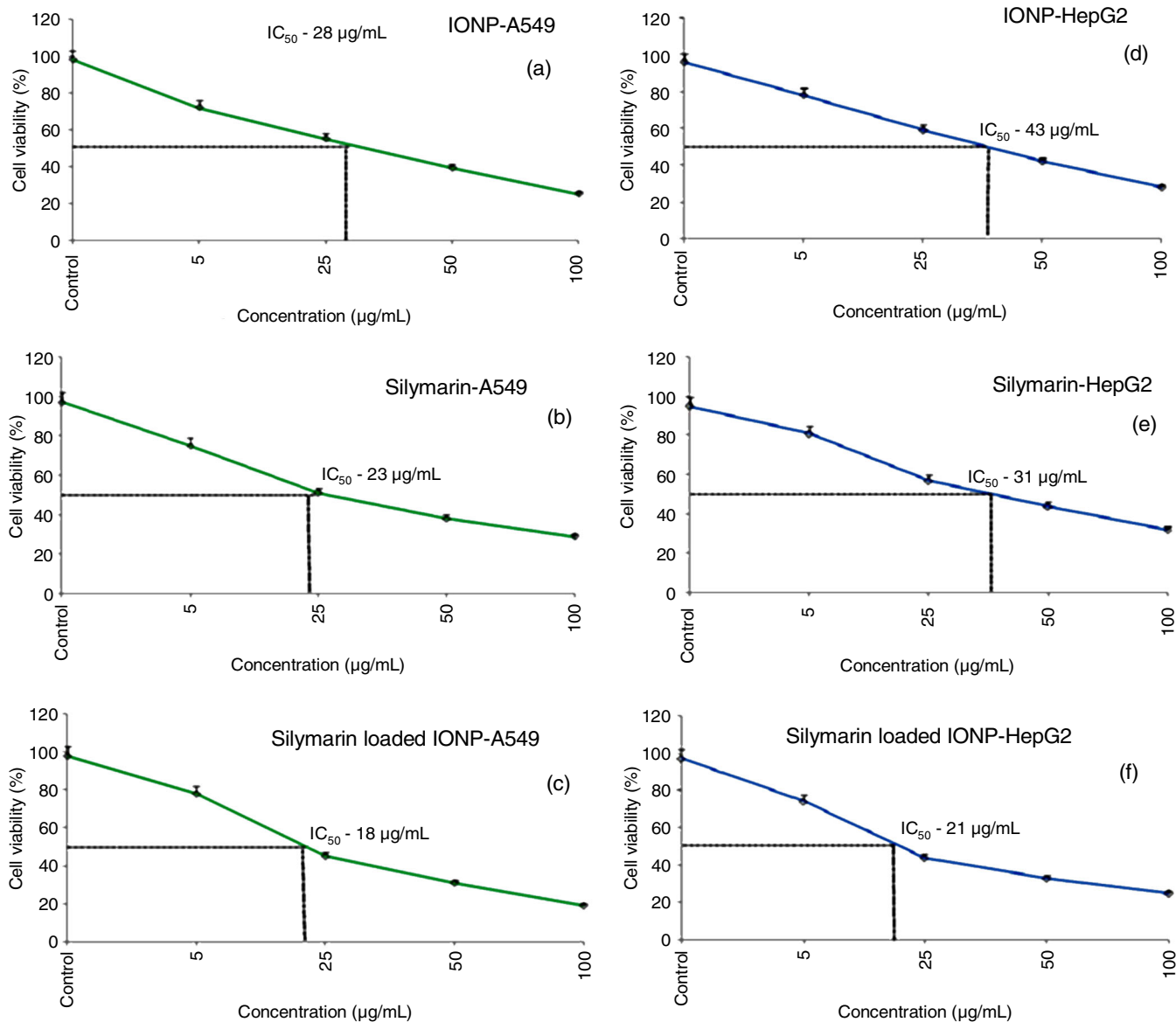

Fig. 6. *In vitro* cytotoxic activity of IONPs, silymarin and silymerin loaded IONPS against A 549 cells (a-c) and HepG2 cells (d-f)

lung (A-549) and liver cancer (HepG2) cells has been studied with MTT assay method. Fig. 6 shows the *in vitro* cytotoxic activity of the synthesized nanoparticles (5-100 µg/mL). The half maxima inhibitory concentration (IC$_{50}$) values of synthesized nanoparticles against the lung and liver cancer cells were calculated and the values are shown in Table-2. The IC$_{50}$ values were found to be 28, 23 and 18 µg/mL for A549 cells and 43, 31 and 21 µg/mL for HepG2 cells for IONPs, silymarin and silymarin loaded IONPs, respectively.

Acridine orange/ethidium bromide staining and DAPI staining fluorescence methods: Acridine Orange penetrated the cell membrane, under a fluorescence microscope, the normal

TABLE-2 CYTOTOXIC ACTIVITY OF IONPs, SILYMARIN AND SILYMARIN LOADED IONPs (µg/mL)		
Sample name	A549	HepG2
IONPs	28 ± 1.5	43 ± 1.5
Silymarin	23 ± 1.0	31 ± 1.5
Silymarin loaded IONPs	18 ± 1.5	21 ± 1.5
IC$_{50}$ – values of respective sample (at 24 h)		

cells were observed as green fluorescence; whereas in apoptotic cells formed as a result of nuclear shrinkage and cell death were observed as orange in colour. Necrotic cells which do not have cell membranes, appeared as red colour fluorescence. Fluore-
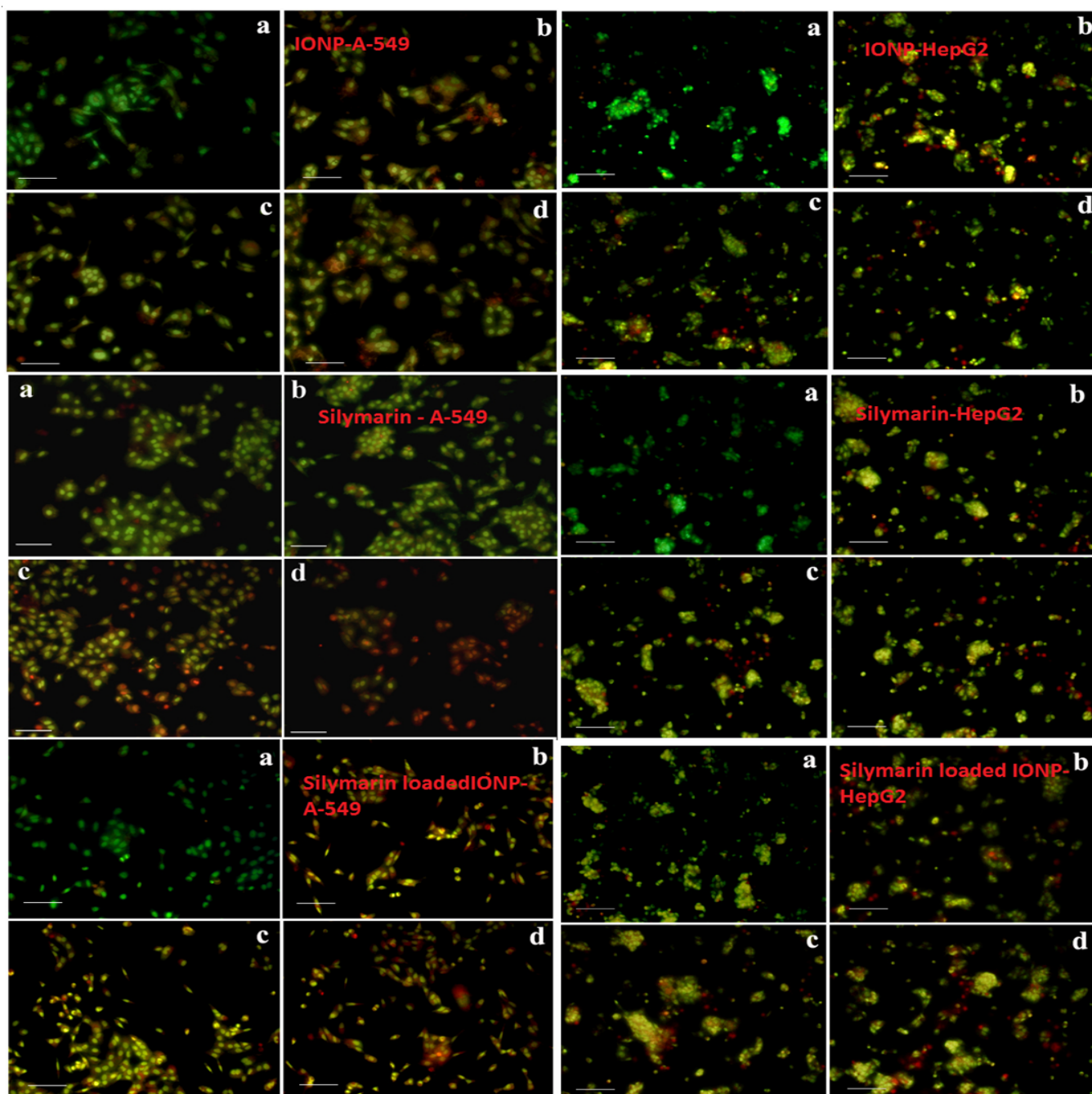
Fig. 7. Fluorescence microscopic analysis of IONPs, silymarin and silymarin loaded IONPs with control (a), 10 µL (b), 25 µL (c) and 50 µL (d) concentrations on A 549 and HepG2 cells

scence microscopic images of A-549 and HepG2 cancer cells in the absence of nanoparticles and in the presence IONPs, silymarin and drug loaded IONPs. From Fig. 7, it is confirmed that the controlled cancer cells did not show any significant changes compared to the treated cells.

Nuclear fragmentation of cancer cells by the IONPs and drug loaded IONPs were analyzed by DAPI (4,6-diamidino-

2-phenylindole) fluorescent staining method. Fluorescence microscopy images of cancer cells after 24 h staining with DAPI in the absence and presence of IONPs, silymarin and drug loaded IONPs are shown in Fig. 8. It was found that the untreated cells shown no significant changes whereas the IONPs and silymarin loaded IONPs treated cells showed bright fetches of fluorescence. This indicates the condensed nuclear fragmen-
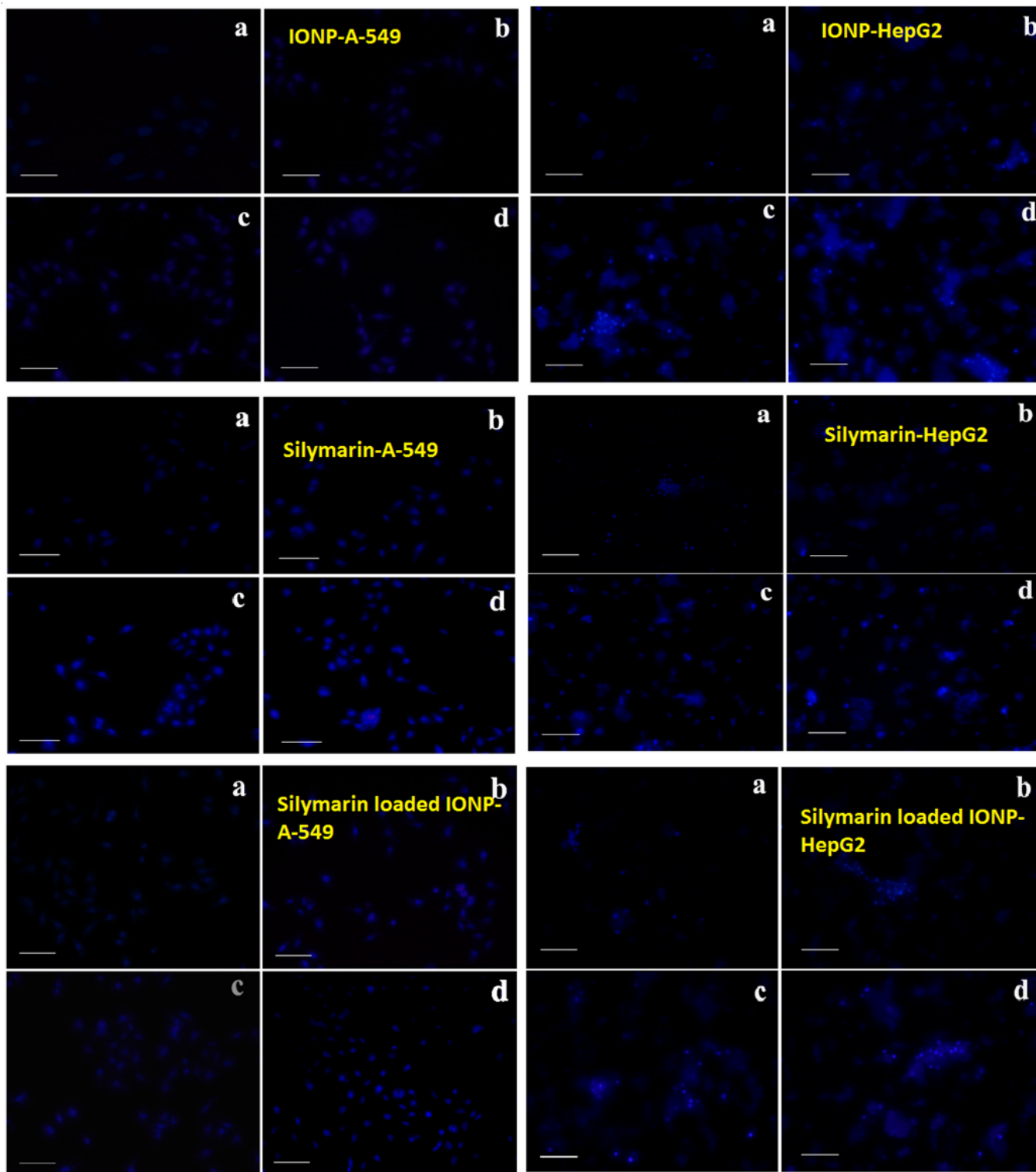

Fig. 8. DAPI analysis of IONPs, silymarin and silymarin loaded IONPs with control (a), 10 µL (b), 25 µL (c) and 50 µL (d) concentrations on A 549 and HepG2 cells

tations due to apoptosis in the treated cancer cells. Thus, from the MTT and fluorescence microscopic analysis results, it can be assertively testified that the silymarin loaded IONPs may be used as potent therapeutic agent for the treatment of lung and liver cancer cells.

Apoptotic cell death analysis: To confirm the cell death by induced apoptosis, flow cytometric studies has been carried out with A-549 and HepG2 cancer cells. The graph has four quadrants namely, Q1-Necrotic cells, Q2-post apoptotic cells, Q3-pre apoptotic cells and Q4-living cells. The results are shown in Figs. 9 and 10; and the data are given in Table-3.

Conclusion

Iron oxide nanoparticles (IONPs) with effective particle size have been prepared for the biomedical applications by a green synthetic route. The anticancer activity of the prepared
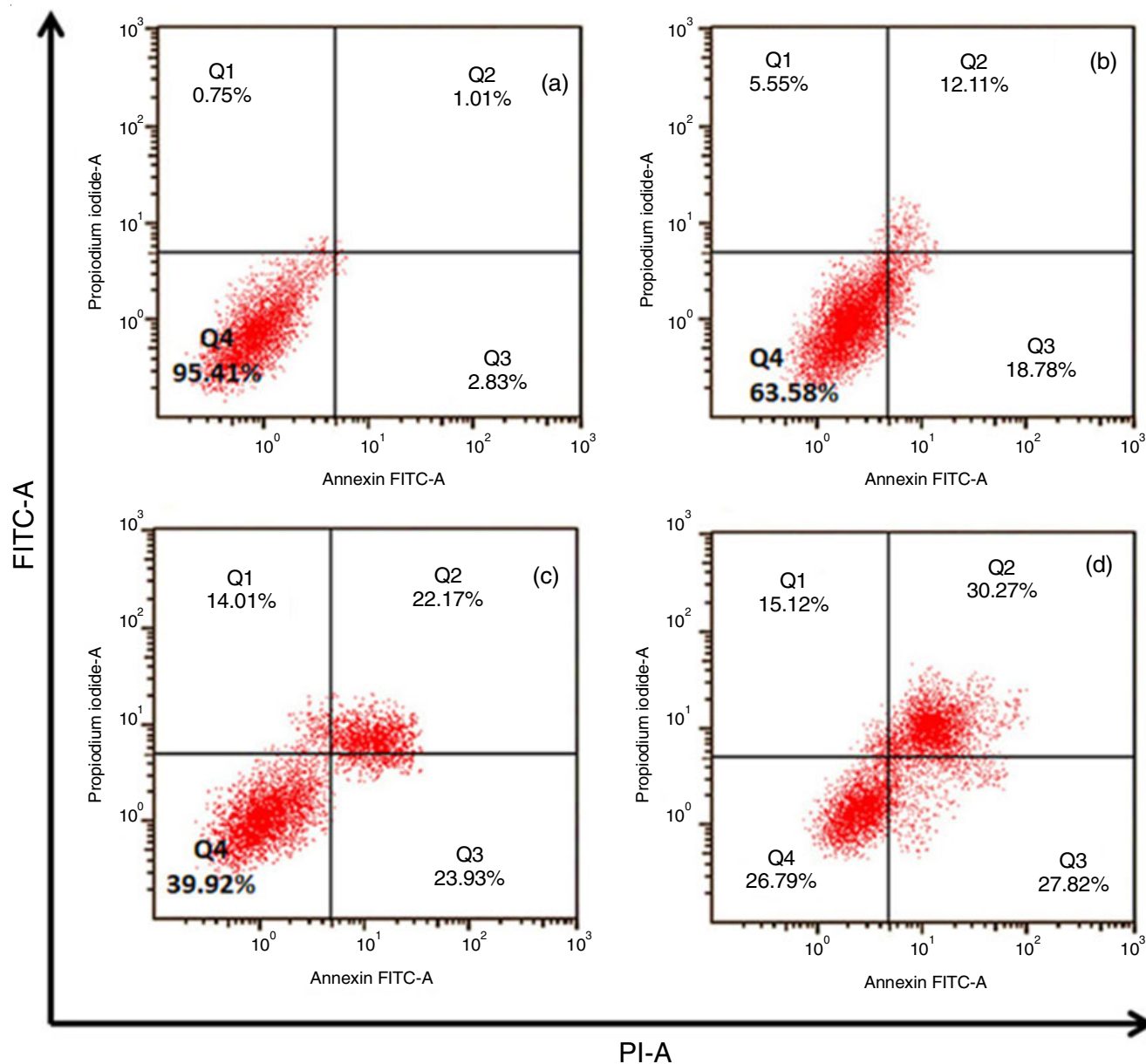

Fig. 9. Flow cytometry analysis of A-549 cells with control (a), IONPs (b), silymarin (c) and silymarin loaded IONPs (d) treated

TABLE-3
QUADRANTS OF NECROTIC, POST APOPTOTIC, PRE APOPTOTIC AND LIVING
CELLS IN A 549 AND HEpG2 CELLS LINES AFTER THE TREATMENT

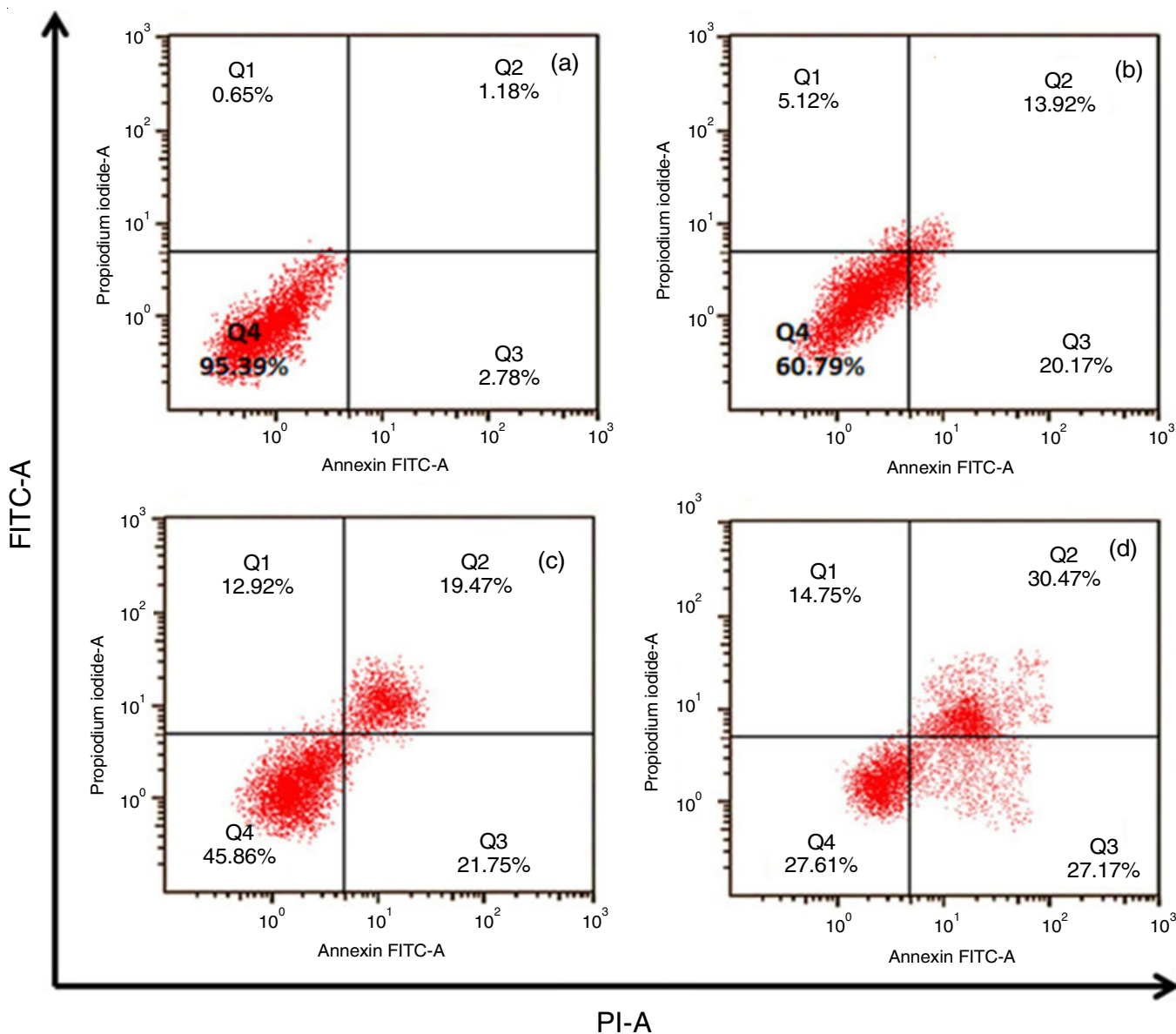| Quadrant	A-549				HepG2			
	Control	10 µg/mL	25 µg/mL	50 µg/mL	Control	10 µg/mL	25 µg/mL	50 µg/mL
Q1	0.75%	5.55%	14.01%	15.2%	0.65%	5.12%	12.92%	14.75%
Q2	1.01%	12.11%	22.17%	30.27%	1.18%	13.92%	19.47%	30.47%
Q3	2.83%	18.78%	23.93%	27.82%	2.78%	20.17%	21.75%	27. 17%
Q4	95.41%	63.58%	39.92%	26.79%	95.39%	60.79%	45.86%	27. 61%

Fig. 10. Flow cytometry analysis of HepG2 cells with control (a), IONPs (b), silymarin (c) and silymarin loaded IONPs (d) treated

IONPs and silymarin loaded IONPs has been studied and compared with the activity of pure drug. The cytotoxicity by MTT assay analysis had given the IC$_{50}$ value of IONPs, silymarin and silymarin loaded IONPs as 28 µg/mL, 23 µg/mL and 18 µg/mL for A 549 cell lines, whereas for HepG2 cell lines the values were 43 µg/mL, 31 µg/mL and 21 µg/mL. The anti-cancer activity of silymarin loaded IONPs showed higher *in vitro* anticancer activity against A-549 lung cancer cells compared to the HepG2 liver cancer cells. Also, the IONPs shows highest inhibition for HEpG2 cells than the A 549 cells. Results from MTT assay were confirmed by the fluorescence microscopic analysis with acridine orange/ethidium bromide and DAPI staining methods. Cell death by the induced apoptosis was further confirmed by flow cytometry. Anticancer effect of silymarin loaded IONPs were due to the targeted delivery of silymarin to the cancer cells by iron oxide nanocarriers. Thus, silymarin loaded IONPs may be assumed as an effective drug delivery agent for anticancer applications.

CONFLICT OF INTEREST

The authors declare that there is no conflict of interests regarding the publication of this article.

REFERENCES

1. A. Moten, D. Schafer, P. Farmer, J. Kim and M. Ferrari, *J. Glob. Health*, **4**, 010304 (2014); https://doi.org/10.7189/jogh.04.010304
2. P.G. Komarov, E.A. Komarova, R.V. Kondratov, K. Christov-Tselkov, J.S. Coon, M.V. Chernov and A.V. Gudkov, *Science*, **285**, 1733 (1999); https://doi.org/10.1126/science.285.5434.1733
3. E. Fernandes, J.A. Ferreira, P. Andreia, L. Luís, S. Barroso, B. Sarmento and L.L. Santos, *J. Control. Release*, **209**, 288 (2015); https://doi.org/10.1016/j.jconrel.2015.05.003
4. F. Dehghani, A.R. Sardarian and M. Esmaeilpour, *J. Organomet. Chem.*, **743**, 87 (2013); https://doi.org/10.1016/j.jorganchem.2013.06.019
5. S. Mancarella, V. Greco, F. Baldassarre, D. Vergara, M. Maffia and S. Leporatti, *Macromol. Biosci.*, **15**, 1365 (2015); https://doi.org/10.1002/mabi.201500142

6. J.S. Kim, T.J. Yoon, K.N. Yu, B.G. Kim, S.J. Park, H.W. Kim, K.H. Lee, S.B. Park, J.K. Lee and M.H. Cho, *Toxicol. Sci.*, **89**, 338 (2006); https://doi.org/10.1093/toxsci/kfj027

7. S. Laurent, D. Forge, M. Port, A. Roch, C. Robic, L. Vander Elst and R.N. Muller, *Chem. Rev.*, **108**, 2064 (2008); https://doi.org/10.1021/cr068445e

8. M.V. Arularasu, J. Devakumar and T.V. Rajendran, *Polyhedron*, **156**, 279 (2018); https://doi.org/10.1016/j.poly.2018.09.036

9. P.L. Pravallika, G.K. Mohan, K.V. Rao and K. Shanker, *Mater. Lett.*, **236**, 256 (2019); https://doi.org/10.1016/j.matlet.2018.10.037

10. H.K. Farshchi, M. Azizi, M.R. Jaafari, S.H. Nemati and A. Fotovat, *Biocatal. Agric. Biotechnol.*, **16**, 54 (2018); https://doi.org/10.1016/j.bcab.2018.07.017

11. K. Flora, M. Hahn, H. Rosen and K. Benner, *Am. J. Gastroenterol.*, **93**, 139 (1998); https://doi.org/10.1111/j.1572-0241.1998.00139.x

12. A.S. Negi, J.K. Kumar, S. Luqman, K. Shanker, M.M. Gupta and S.P. Khanuja, *Med. Res. Rev.*, **28**, 746 (2008); https://doi.org/10.1002/med.20115

13. S. Arsalani, E.J. Guidelli, J.F.D.F. Araujo, A.C. Bruno and O. Baffa, *ACS Sustain. Chem.& Eng.*, **6**, 13756 (2018); https://doi.org/10.1021/acssuschemeng.8b01689

14. M. Mahdavi, M. Ahmad, M. Haron, F. Namvar, B. Nadi, M. Rahman and J. Amin, *Molecules*, **18**, 7533 (2013); https://doi.org/10.3390/molecules18077533

15. S. Amala Jayanthi, A. Muthuvinayagam, T. Manovah David and P. Sagayaraj, *Der Pharma Chem.*, **4**, 1535 (2012).

16. M. Khalkhali, S. Sadighian, K. Rostamizadeh, F. Khoeini, M. Naghibi, N. Bayat and M. Hamidi, *Nanomed. J.*, **2**, 223 (2015).

17. F.M. Alminderej, *Arab. J. Chem.*, **13**, 3672 (2020); https://doi.org/10.1016/j.arabjc.2019.12.005

18. K. Kavithaa, M. Paulpandi, T. Ponraj, K. Murugan and S. Sumathi, *Karbala Int. J. Modern Sci.*, **2**, 46 (2016); https://doi.org/10.1016/j.kijoms.2016.01.002

19. A. Radoñ, P. Wlodarczyk, A. Drygala and D. Lukowiec, *Appl. Surf. Sci.*, **474**, 66 (2019); https://doi.org/10.1016/j.apsusc.2018.05.045

20. S. Latha, P. Selvamani, T.K. Pal, J.K. Gupta and L.K. Ghosh, *Ancient Sci . Life*, **26**, 19 (2006).

21. T.Y. Suman, D. Elumalai, P.K. Kaleena and S.R.R. Rajasree, *Ind. Crops Prod.*, **47**, 239 (2013); https://doi.org/10.1016/j.indcrop.2013.03.010

22. T. Heimburg, J. Schu-nemann, K. Weber and N. Geisler, *Biochemistry*, **38**, 12727 (1999); https://doi.org/10.1021/bi983079h

23. A.A. Zahir and A.A. Rahuman, *Vet. Parasitol.*, **187**, 511 (2012); https://doi.org/10.1016/j.vetpar.2012.02.001